Use of Retaining Walls in Shallow Geothermal Energy Systems

Duarte Nuno de Jesus Silva

Instituto Superior Técnico, Universidade de Lisboa, Portugal (2020)
duarte.j.silva@tecnico.ulisboa.pt

A B S T R A C T

Shallow geothermal energy has been used to provide renewable thermal energy to residential and commercial buildings, mainly by means of ground-source heat pump systems that leverage the soil heat storage potential. One main drawback of these systems is the high capital cost associated with their construction that can be significantly reduced if the heat exchanger loops are incorporated into piles, retaining walls and tunnel linings, being therefore classified as thermally-activated structures or energy geostructures. While energy piles are the most common application, in the last decade the interest around energy walls has increased. However, there are still some knowledge gaps regarding the thermal behaviour of energy walls that due to their complexity require numerical analyses to asses their thermal performance. Therefore, a thermal analysis of a diaphragm energy wall was undertaken in the finite element software FEFLOW. The software response was validated not only against a set of available field data but also against an existing numerical study, revealing a good agreement with both sets of data, which allowed to establish some guidelines for the assembly of the subsequent parametric study. The parametric study focused on the impact of the ground (soil thermal conductivity), wall geometry, heat exchanger loop layout, interior and exterior environment and thermal load on the heat transfer rate. The results show that the conditions in the excavated space have a significant impact on the heat transfer rate of energy walls, followed by the wall geometry and the soil thermal conductivity.

Keywords: energy geostructures; energy walls; ground source heat pump systems; geothermal energy; renewable energy;

1 Introduction

Global energy demand has seen an exponential increased in the past decades due to the growing population and the quest for a better quality of life, with most of that energy demand being fulfilled by energy sources with great impact on the environment, like fossil fuels. Since it is expected that energy consumption will continue to rise, it is essential to shift from coal, oil, and natural gas to renewably energy sources, even with energy production at the local level. As a result, shallow geothermal energy has great potential to become one of the most relevant energy sources since it can be produced locally, is widely available and is sustainable.

Shallow geothermal energy (SGE) is characterized by depths less than about 150 m and lower temperatures (typically <30°C) , which with the aid of a heat pump can be used to provide heating and cooling [1], to residential and commercial buildings, as well as infrastructures, like metro stations. The energy source of SGE systems is always available which means that the systems availability is independent from the time of the day or the weather conditions. Moreover, the ground exhibits an almost constant temperature throughout the year, with only the first 10-15 m showing a seasonal temperature change due to surface conditions [2] below a few metres of depth, which makes the system independent from solar energy gains. In the case where groundwater flow is absent, the ground can act as a heat storage, accepting excessive heat in the summer and releasing that heat in the winter. Usually, the system is comprised by a primary circuit, the heat exchanger loop that exchanges heat with the ground, and a secondary circuit, that exchanges heat with the building, that are connected via a ground source heat pump (GSHP) that increases the system efficiency, as the differences in temperature between the source and the sink, the ground and the building in heating mode, respectively, are very small in SGE systems.

In fact, the efficiency of the ground-source heat pump can be evaluated by the ratio between the extracted energy and the energy spent for operation, also referred to as the coefficient of performance (COP). The COP coefficient is directly dependent from the source and sink temperatures (higher values are achieved for lower temperature differences between those), so a GSHP do not have a fixed COP value. Due to the variability between different systems, an alternative performance metric that takes into consideration the whole system can be defined. This metric is referred to as the seasonal

performance factor (SPF) [3], and while it considers the GSHP efficiency, it also considers the energy consumption from the primary and secondary circuits (usually circulating pumps) and from additional energy sources (back-up heaters or auxiliary cooling units). Reports from GSHP field trials in the UK [4] and from GSHP monitored systems in Germany [5] show that the average SPF value is higher in GSHP systems than in air source heat pump (ASHP) systems, and that the former is usually combined with underfloor heating systems as a secondary circuit, leveraging the higher achievable efficiencies due to the lower required temperatures.

There are multiple applications of GSHP systems with the most common being horizontal ground loops, vertical ground loops, and energy geostructures. Foundation elements such as slabs, retaining walls and piles, and underground structures like tunnels can incorporate heat exchangers without losing their main structural purpose, therefore, assuming a dual function.

This study focuses on the application of thermally activated diaphragm walls, also referred to as energy walls, in shallow geothermal energy systems. There are some reports regarding monitoring data and field tests of energy walls [6]–[9] as well as system implementation and construction [10], [11]. Numerical studies have been performed to try to asses the thermal behaviour of energy walls and the parameters that impact the heat transfer rate most the [12]–[15].

2 Parametric Study

Based on considerations from previous works, a parametric study was assembly. The thermal analyses were performed through the finite element software FEFLOW [16]. The general methodology for establishing the 3D model in FEFLOW goes as follows: To generate the finite element mesh, a two-dimensional (2D) vertical cross-section is defined first, according to the model boundaries and wall geometry, along with a line positioned on the location of the heat exchanger loop, to “impose” a continuous alignment of mesh element edges. Subsequently, the mesh is generated using triangular elements, according to the element dimensions and defined refinement areas. Then the 2D model is converted to a 3D model through a layered configuration in which a defined spacing is applied to each layer. The spacing and the number of layers describe not only the model width but also the degree of discretisation in the third dimension.

Then, the triangular mesh elements are transformed into prismatic six-node 3D elements that are vertically aligned and form a layer. In FEFLOW terminology, a slice is a set of 2D mesh elements while a layer is a set of 3D elements located between two slices. After the 3D model generation, the problem class is defined, i.e. it is specified as a saturated groundwater medium, including only the transport of heat in a transient state.

Following these steps, the remaining parameters can be assigned: initial temperature and material thermal properties are assigned to the elements while boundary conditions (BC) are assigned to the element nodes. Lastly, the heat exchanger loop geometry is implemented via 1D special elements called “Discrete Features”, assigned to the edges of the mesh elements. Although these elements neglect the HDPE pipe wall resistance, authors report insignificant temperature output errors [12]. Additionally, and given that the standard geometry for 1D discrete features is not the submerged circular cross-section, corrections must be adopted. These corrections are assigned into the software via the hydraulic aperture, b, for the Haggen-Poiseuille law [16]. The software will then compute the true hydraulic radius of the heat exchanger pipes via the hydraulic aperture, b, and the geometrical input parameter, the cross-section area, *A*. Additionally, to impose a fluid flow in the pipes, the fluid velocity value is assigned to the inlet and outlet nodes via a fluid-flux BC.

2.1 Geometry

The diaphragm walls geometry presents some variability, mainly depending from the purpose of the structure in which they are implemented. Table 1 summarizes the diaphragm wall geometries of similar studies where is possible to see wall depths (Dw) between 15 m and 38 m as well as wall panel thicknesses (Tw) between 0.8 m and 1.2m. The excavation depth (De) and the panel width (W) are also presented.

Figure 1a) shows the general wall geometry considered in the parametric study, as the parameters that need to be defined. Therefore, to assess the impact of the geometry on the thermal performance of the wall, three different wall geometries were defined, as presented in Table 2. The aim was to reproduce the geometry for three implementation scenarios: the first and the second as an underground carpark or building basement and the third as an underground metro station.

Table 1 - Summary of diaphragm wall geometries.

Ref.	Dw [m]	De [m]	W [m]	Tw [m]
[10]	36.0	24.0	3.3	0.8
[8]	38.0	18.5	2.25	1.0
[7]	15.2	10.8	2.4	0.5
[12]	20.0	10.0 – 16.0	1.5	0.8 – 1.2
[17]	15.5	9.5	2.5	0.8

Table 2 - Wall geometry parameters assumed in the parametric study.

Geometry	Dw [m]	De [m]	W [m]	Wall surface area, A_w [m²]	Tw [m]	Ts [m]
G1	15	10	1.6	24	0.6	0.6
G2	25	20	1.6	40	0.9	0.9
G3	35	30	1.6	56	1.2	1.2

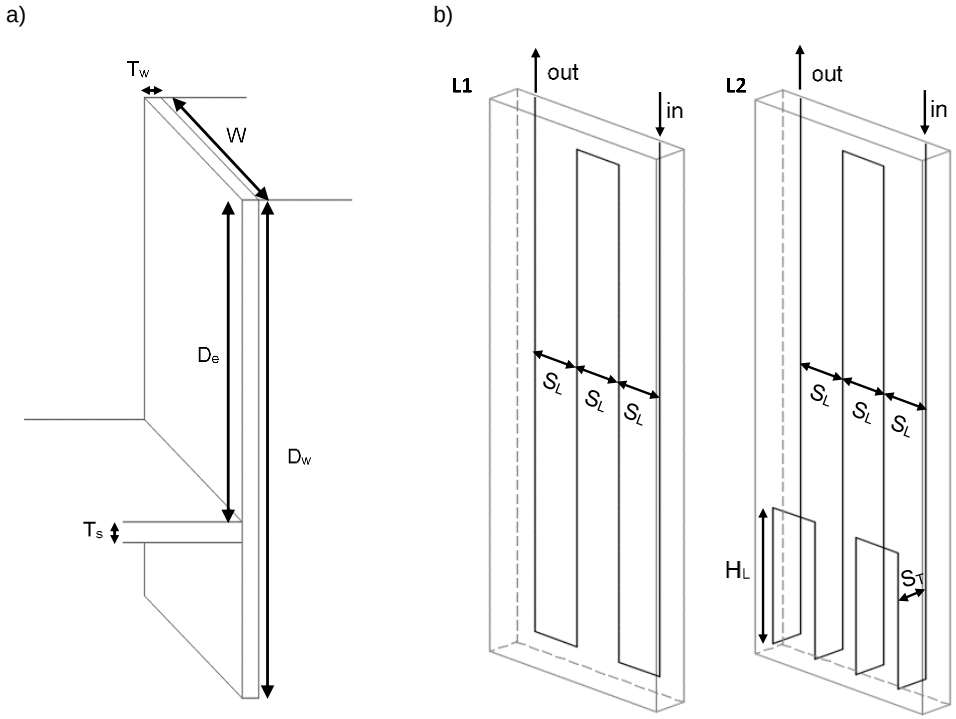

Figure 1 - Wall and heat exchanger loop geometry parameters.

Regarding the heat exchanger loop, two different layouts were defined (Figure 1 b)) to evaluate the increase in heat transfer rate from a layout with higher contact area with the ground. A longitudinal spacing, S_L, of 0.4 m was adopted considering that there is no significant thermal performance increase from adopting a spacing lower than 0.3 m [18], [19]. A concrete cover to the pipes, C, of 0.1m was also adopted as well as a distance of 1 m from the horizontal pipe branch at the top and the top boundary. The transverse spacing between vertical pipe branches, S_T, and the height of the loop on the embedded part of the wall, H_L, on the heat exchanger loop L2, are defined as:

$$S_T = T_W - 2C \quad (1)$$

$$H_L = D_W - D_e - T_S - 0.5 \quad (2)$$

The exterior diameter of the heat exchanger pipes, d_o, was fixed at 25mm, with a wall thickness, t_{pw} , of 2mm, which correlates to an inner diameter, d_i, of 21mm and a cross sectional area, A, of 346.36 mm².

The material properties that need to be defined are those for the soil, geostructure and heat carrier fluid. These were defined as bulk values. Table 3 lists the thermo-physical properties of the materials assumed for the parametric study. The soil thermal conductivity, λ_S, will assume values of 1.0, 2.0 or 3.0 W/m K, depending on the run, to evaluate the impact of this soil parameter in the thermal performance of the system. All of the other material parameters are constant throughout the performed analyses. While the concrete thermal conductivity could become an important parameter in the long term [12], it was not considered in the parametric analysis.

2.2 Initial temperatures and boundary conditions

The initial soil and wall temperatures were defined as 17ºC, considering the average air temperature in Lisbon [20]. Given that the simulation length of the analyses was set to 3 years (1095 days), a set

Table 3 - Material Properties assumed in the parametric study.

	Soil	Geostructure	Heat carrier fluid
Bulk density ρ [kg m^{-3}]	2000	2500	1000
Bulk specific heat capacity c [J kg^{-1} K^{-1}]	1000	900	4200
Bulk volumetric heat capacity $c\rho$ [MJ m^{-3} K]	2.0	2.25	4.2
Bulk thermal conductivity λ [W m^{-1} K^{-1}]	1.0/2.0/3.0	2.0	0.6

Table 4 - Temperature Boundary conditions for the parametric study.

	Assigned boundary	Case	Temperature [ºC]	Equation
Inlet	Inlet node	**In_1**	**17 ± 10**	$T_{in}(d) = 17 + 10\sin\left(2\pi d/365\right)$
		In_2	20 ± 7	$T_{in}(d) = 20 + 7\sin\left(2\pi d + 25.7294 \times 2\pi/365\right)$
		In_3	14 ± 7	$T_{in}(d) = 14 + 7\sin\left(2\pi d + 25.7294 \times 2\pi/365\right)$
Interior space BC	Slab and wall surface	**Int_1**	**17 ± 3**	$T_{int}(d) = 17 + 3\sin\left(2\pi d/365\right)$
		Int_2	23 ± 5	$T_{int}(d) = 23 + 5\sin\left(2\pi d/365\right)$
Exterior BC	Top boundary	**Ext_1**	**17 ± 6**	$T_{ext}(d) = 17 + 6\sin\left(2\pi d/365\right)$

of varying temperature BC were established. Table 4 presents the temperature ranges of the inlet, interior space and exterior BC, the boundaries in which will be assigned and the equation that describes the sinusoidal profile. The values in bold refer to the baseline values, while the others will introduce variations on the interior space and on the thermal load imposed by the inlet temperature. Figure 2 presents the yearly temperature profiles for the inlet temperature and BC considered.

Additionally, the boundaries with no BC assigned are adiabatic by default, which means that no heat flux will occur through them and the temperature at those nodes can change freely. These boundaries were checked to be far enough from the wall to not impact the thermal performance. A fluid flux BC was assigned to the inlet and outlet nodes to impose a fluid velocity, v, of 0.6 m/s in accordance with [8], [12], [17].

Table 5 summarises the combination of parameters in each simulation run of the baseline analysis, defined in terms of the inlet and boundary conditions' temperature profiles presented in Table 4 in bold. A case name was defined for each simulation run, containing the wall geometry, heat exchanger layout and the soil thermal conductivity considered for the run, and assuming the baseline values for the inlet and boundary conditions temperature profiles mentioned previously, thus making it easy to identify and compare the results. The presented cases will serve as reference to additional simulations .

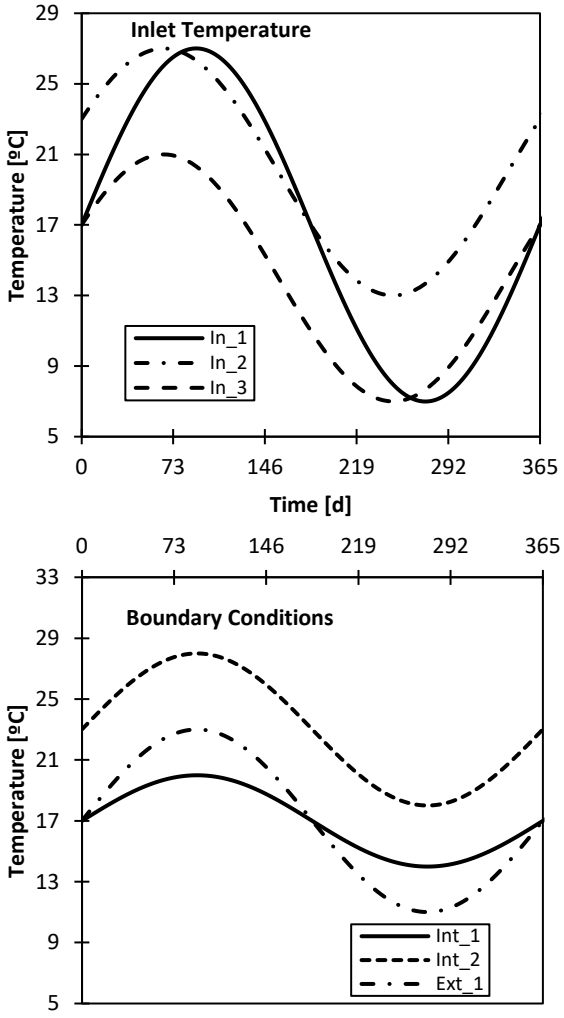

Figure 2 - Yearly temperature profiles.

Table 5 - Baseline analysis cases details.

Wall Geometry	Heat Exchanger Layout	BC	λ_S [W m^{-1} K^{-1}]	Case
G1	L1	Baseline	1.0	G1_L1_1.0
			2.0	G1_L1_2.0
			3.0	G1_L1_3.0
	L2	Baseline	1.0	G1_L2_1.0
			2.0	G1_L2_2.0
			3.0	G1_L2_3.0
G2	L1	Baseline	1.0	G2_L1_1.0
			2.0	G2_L1_2.0
			3.0	G2_L1_3.0
	L2	Baseline	1.0	G2_L2_1.0
			2.0	G2_L2_2.0
			3.0	G2_L2_3.0
G3	L1	Baseline	1.0	G3_L1_1.0
			2.0	G3_L1_2.0
			3.0	G3_L1_3.0
	L2	Baseline	1.0	G3_L2_1.0
			2.0	G3_L2_2.0
			3.0	G3_L2_3.0

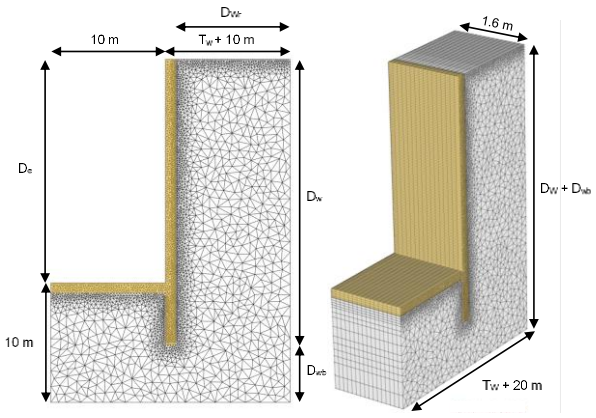

Figure 3 - Adopted mesh and model geometry.

Figure 3 shows the adopted mesh and model geometry. A sensitivity analysis was performed in both parameters to assess their impact on the heat transfer rate.

3 Results

3.1 Baseline analysis results

The baseline analysis was defined in Table 5, comprising the geometries, the soil thermal conductivities and the heat exchanger layouts previously defined. The outlet temperature evolution for all of the cases describes, as expected, the sinusoidal behaviour imposed by the inlet and boundary condition temperature profiles (Figure 2), with small outlet temperature differences between them. These small differences are more visible when the results are presented in terms of heat transfer rate per wall surface area, q [W m^{-2}], computed through the following equation:

$$q = {}^{Q}/_{A_w} \quad (3)$$

Considering Q as:

$$Q = mc_w\,(T_o - T_i) \quad (4)$$

Note that in accordance with equation (4), positive heat transfer rates refer to the heating operation mode, as outlet temperatures are higher than inlet temperatures, and negative heat transfer rates refer to the cooling operation mode, as outlet temperatures are lower than inlet temperatures. Figure 4 shows the heat transfer rate evolution for the period comprising the third year of simulation, from 730 d to 1095 d. Although only the 2.0 W/m K soil thermal conductivity cases are presented in Figure 4, a similar behaviour was identified for the 1.0 W/m K and 3.0 W/m K soil thermal conductivity cases.

3.2 Influence of soil thermal conductivity, wall and heat exchanger geometry

The first parameters to be discussed are the soil thermal conductivity, wall geometry and heat exchanger layout. This analysis is based on the results of the baseline analysis cases, alongside an additional simulation based on case ***G2_L1_2.0***, with a higher embedded depth of 10 m. The distinguished parameter in relation to all of the other cases is the total wall depth that goes from 25 m to 30 m, therefore the case name ***G2_L1_2.0_30*** adopted for this additional

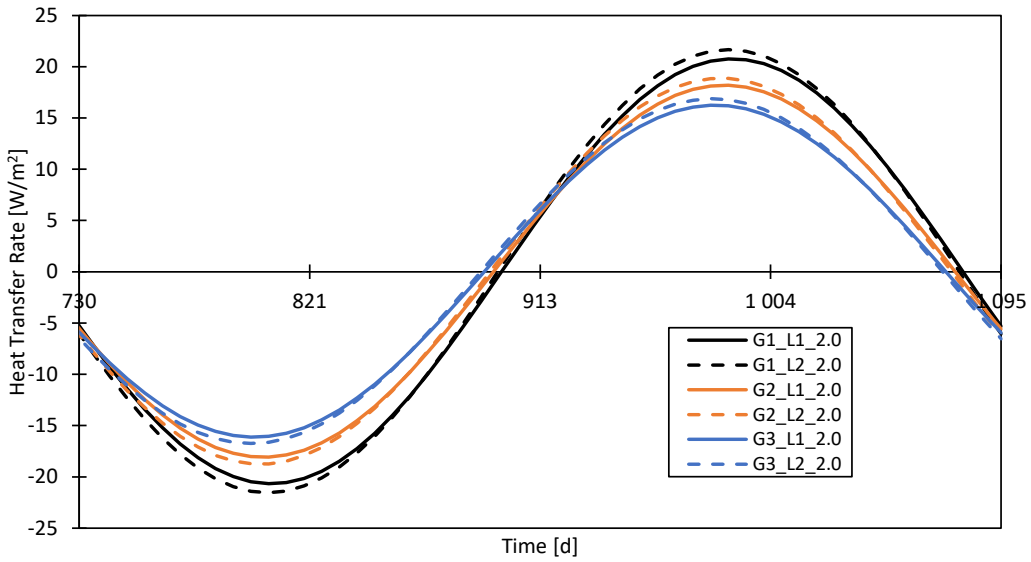

Figure 4 - Baseline analysis heat transfer rate during the third year of simulation.

simulation. To compare the heat transfer rates from the different geometries, a new parameter, D_b, the embedded depth of the wall below excavation level, was defined, as:

$$D_b = D_w - D_e \quad (5)$$

The relationship curves between the heat transfer rate and the soil thermal conductivity are presented in Figure 5, therefore the case names omit this parameter. The relationship curves between the heat transfer rate and the excavation to embedded depth ratio are presented in Figure 6, in which the case names omit the geometry type, as the relationship is dependent on the ratio between De and Db.

As expected, the highest heat transfer rates are achieved for the highest values of soil thermal conductivity. An almost linear relationship is observed between the soil thermal conductivity and the heat transfer rate, in all of the geometries and heat exchanger layouts. For heat exchanger layout L1 specifically, a heat transfer rate increase of 11.1%, 11.3% and 12.5% (heating) and of 11.0%, 11.1% and 12.3% (cooling) is observed for geometries G1, G2 and G3, respectively, through doubling the soil thermal conductivity, translating to an average increase of 11.6% and 11.4% for heating and cooling, respectively. Furthermore, the 50% increase in soil thermal conductivity, from 2.0 W/m K to 3.0 W/m K, translates to an increase in heat transfer rate of 7.4%, 7.5% and 8.1% (heating) and of 7.4%, 7.6% and 8.2% (cooling) for geometries G1, G2 and G3, respectively, resulting in an average increase of 7.7% for both heating and cooling.

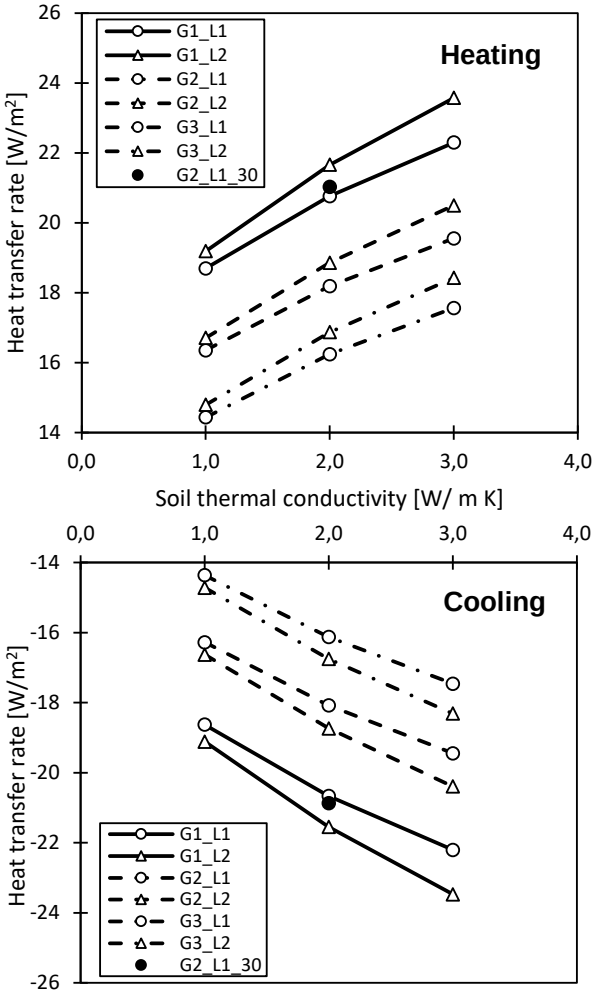

Figure 5 - Effect of soil thermal conductivity, wall and heat exchanger geometry.

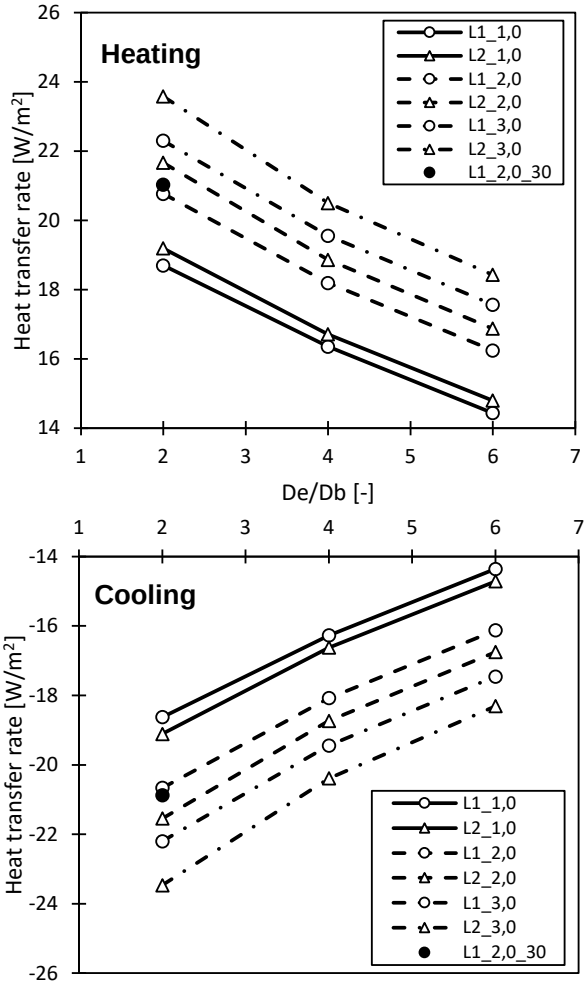

Figure 6 - Effect of soil thermal conductivity, wall and heat exchanger geometry.

A similar behaviour is observed for the geometries combined with the heat exchanger layout L2, translating to an average heat transfer rate increase of 13.3% and 13.1% for heating and cooling respectively, from doubling the soil thermal conductivity, and an average increase of 8.9% and 9.0% for heating and cooling respectively, from 2.0 W/m K to 3.0 W/m K. As the heat exchanger layout L2 has a higher area in contact with the ground, the increase in soil thermal conductivity results in a higher increase of heat transfer rate.

The heat exchanger layout, also impacts the heat transfer rate but to a lesser degree than the soil thermal conductivity. The influence increases, as the soil thermal conductivity increases. In fact, an average increase in heat transfer rate of 2.4% (1.0 W/m K), 4.0% (2.0 W/m K) and 5.2% (3.0W/m K) is observed between the heat exchanger layout L1 and L2 in heating mode, while an average increase of 2.4% (1.0 W/m K), 3.9% (2.0 W/m K) and 5.2% (3.0 W/m K), between the heat exchanger layout L1 and L2, is observed in cooling mode. An average increase of 20.1% (L1) and 23.3% (L2) is observed from 1.0 W/m K to 3.0W/m K. Although the direct comparison of results could be erroneous due to the high variability in the parameters used, [15] reports results for a similar set of heat exchanger layouts and wall geometry (De/Db = 2.1), and a soil thermal conductivity of 2.2 W/m, that show a 5.0% increase in the heat transfer rate per square metre of wall from a layout only on one side of the embedded part of the wall (like layout L1) to a layout on both sides of the embedded part of the wall (like layout L2).

Regarding the wall geometry, the results show that as the depth of the wall increases, from G1 to G3 or from De/Db=2 to De/Db=6, the heat transfer rate per square metre of wall decreases. However, this trend is counteracted by the case ***G2_L2_30*** / ***L2_2.0_30*** in which a total wall depth of 30 m results in a similar heat transfer rate to that of a 25 m total depth wall (G1 or De/Db=2). Namely, it is possible to conclude that the case ***G2_L1_30*** reveals a similar heat transfer rate to ***G1_L1*** for a soil thermal conductivity of 2.0W/m K, as seen in Figure 5, and the case ***L1_2.0_30*** reveals a similar heat transfer rate to ***L1_2.0*** for a De/Db ratio of 2, as seen in Figure 6. This indicates that the wall geometry, specifically the ratio between the exposed part and the embedded part of the wall, plays an important role in the thermal output of the system. Although this geometry was only tested with a soil thermal conductivity of 2.0 W/m K and the heat exchanger layout L1, a similar behaviour is expected in the other cases considered, i.e. an almost linear relationship with the soil thermal conductivity and the De/Db ratio, with an offset from the results of geometry type G2, if subject to the same parameter variations. This is due to a higher embedded depth that increases the ground contribution to the resulting heat transfer rate.

3.3 Influence of interior space

The boundary condition of the exposed wall face was changed from a variable temperature BC (exterior air temperature) to either an adiabatic BC or a convective heat transfer BC, representing case ***G1_L1_2.0_C*** and ***G1_L1_2.0_A***, respectively. In the case of the convection BC, a variable temperature BC has to be combined with a heat transfer BC. The convective heat transfer coefficient, h, has to be defined, and a value of 10 W/m^2 K was adopted after [14], to simulate moderate air-speeds (0.5 to 2 m/s) inside the excavation space.

Figure 7 presents the results for the two considered boundary conditions alongside the heat transfer rate results of case ***G1_L1_2.0***

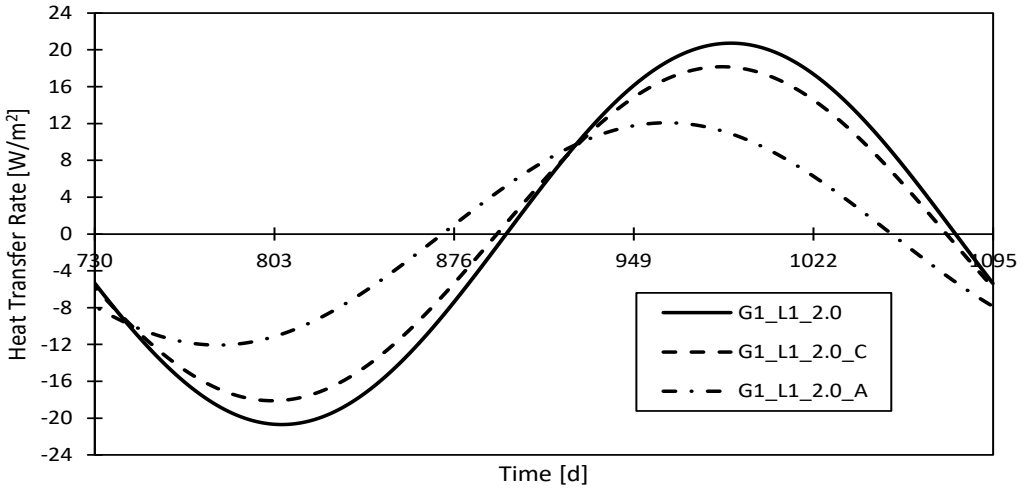

Figure 7 - Interior space BC analysis: results for the third year of simulation.

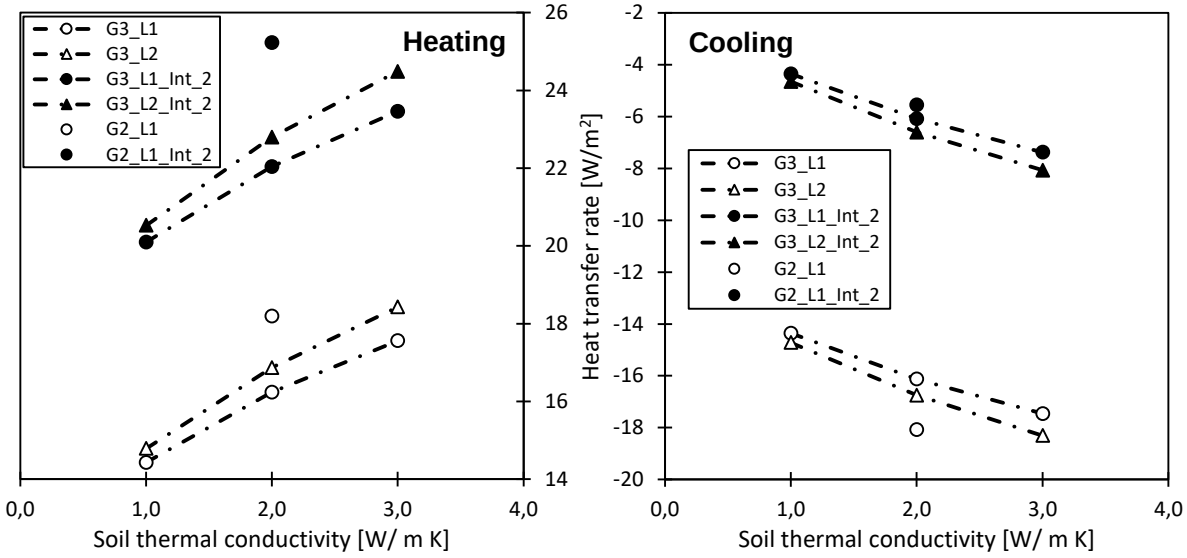

Figure 8 - Heat transfer rate results for the interior space analysis

(Variable temperature BC). As expected, the convective boundary condition heat transfer rate is in between the two extremes, imposed by the temperature and adiabatic boundary conditions. The results of the adiabatic boundary condition show that almost 42% of the heat output is due to the heat exchange between the wall and the excavated space. On the other hand, the difference between assuming very large air-speeds and moderate air-speeds on the wall surface, i.e. between ***G1_L1_2.0*** and ***G1_L1_2.0_C***, results in a loss of efficiency of almost 13%.

An additional set of simulations was established to evaluate the system response to a warmer interior space. Therefore, all of the cases of geometry type ***G3*** and the case ***G2_L1*** (see Table 5) were considered. The interior BC was changed to the Int_2 BC, defined in Table 4. The results in terms of heat transfer rate per square metre of wall are presented in Figure 8, alongside the results of case ***G3_L1***, the reference case with the interior BC Int_1. As shown, there is a significant increase in the heat transfer rate in heating mode and, conversely, a significant decrease of performance in cooling mode. In fact, the cooling provided by the system results from the previous heating operation in which the heat extracted lead to a low temperature field around the wall. That allows for a short cooling period as soon as the inlet temperature increases again, that ceases when the wall and the soil around it reach a thermal equilibrium with the inlet temperature. Consequently, it is possible to conclude that the cooling provided is only due to the storage capacity of the wall and soil and that the interior space do not contribute in a positive

way to it. Actually, once the wall is colder than the interior boundary condition, the interior space is contributing in a negative way to the cooling performance of the wall. The differences between these set of simulations, with interior BC Int_2, and the baseline analysis simulations, shows an average heat transfer rate increase between 35.6% and 38.7%, in heating mode, and an average heat transfer rate decrease between 61.6% and 69.3%, in cooling mode. It is also noticeable that as the soil thermal conductivity increases, the percentage differences to the baseline analysis decrease. Once again, this is due to the higher contribution of the soil to the heat performance of the system.

Two of the previous considered cases had the simulation time extended to 10 years to check if there was some degradation in the heat transfer rate imposed by the warmer interior space since the average value of the BC Int_2 is higher than all of the other imposed temperatures. However, no significant drop in thermal performance was observed. With this result, the temperature profiles at 3 m and 25m depth were checked, from the wall face to the right boundary, both with and without the geothermal system activated for the case ***G3_L1_2.0_Int_2***.

The temperature profiles are presented in Figure 9 in which is possible to conclude that when the geothermal system is activated, the temperature profiles are stable and remain at the temperature registered for the first year of simulation, conversely to what is observed when the geothermal system is deactivated. Therefore, , the excessive heat from the interior environment is being absorbed by the heat exchanger loop, which prevents the system saturation in the long term.

3.4 Influence of top boundary condition

An additional set of simulations was defined based on geometry types ***G1***, ***G2*** and ***G3***, the heat exchanger layout ***L1*** and a soil thermal conductivity of ***2.0*** W/m K to evaluate how the top BC impacts the heat transfer rate. Namely, if the

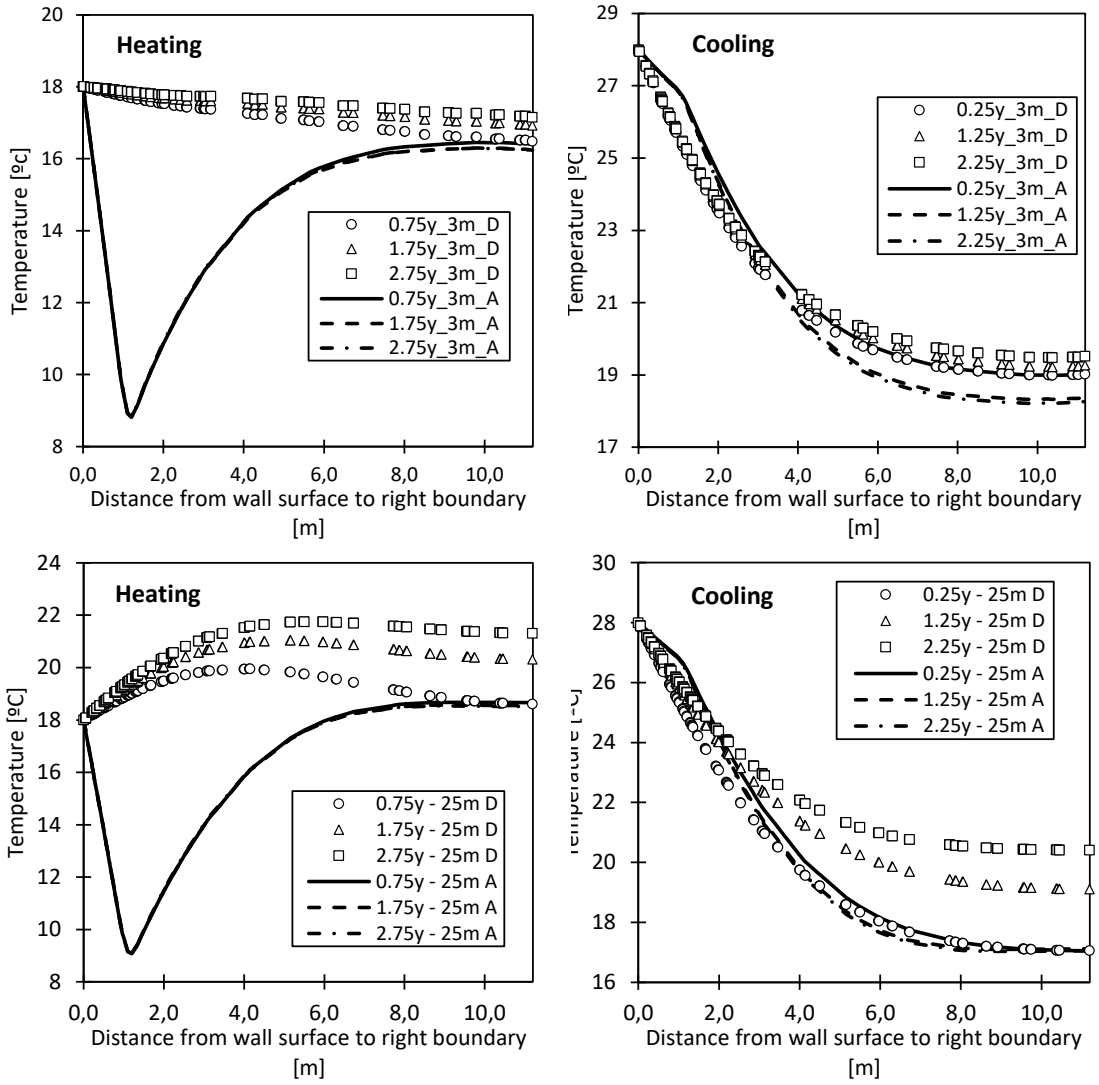

Figure 9 - Temperature profiles at 3 m and 25 m depth for case G3_L1_2.0_Int_2. D and A refer to geothermal system deactivated and activated, respectively.

top BC is somehow responsible for the higher heat transfer rate values computed for the geometries with lower total depth, as it is expected to impact those in a larger degree than it does to the deeper geometries Therefore, the top BC was changed to an adiabatic BC, with the case name ***L1_2.0_Atop***. As Figure 10 shows, the influence on the heat transfer rate is low, with the De/Db ratio of 2 showing the highest difference (0.92%). Similar results were obtained for the cooling period. As a result, the higher surface area of the deeper geometries, as well as the depth, seems to be the factors that explain why normalising the exchange power (Q) by the wall area or depth, results in lower heat transfer rates, as the higher values of those parameters overcome the gain in exchange power of the biggest wall geometries.

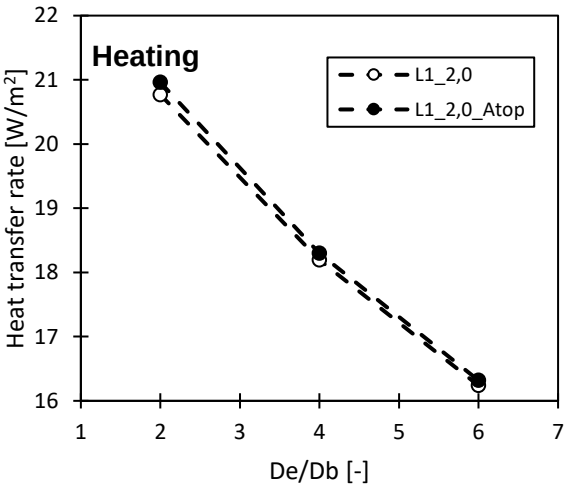

Figure 10 - Results of top BC analysis.

3.5 Influence of inlet temperature

An unbalanced thermal load was imposed to the system by changing the inlet temperature assigned to the case ***G2_L1_2.0***. The two new inlet temperature profiles, ***In_2*** (heating dominant) and ***In_3*** (cooling dominant) were defined in Table 4. . As a result, the case ***G2_L1_2.0_In_2*** shows a 3.5%, 2.2% and 1.5% increase in hat transfer rate, in heating mode, for the first, second and third year of simulation. As the thermal load is heating dominant, the cooling performance is much lower than that of case G2_L1_2.0 (-67.3%, -60.9% and -59.9% for the first, second and third year of simulation). The case ***G2_L1_2.0_In_3*** shows a high heat transfer rate value at early simulation time due to the high difference in temperature between the inlet and the outlet, therefore not being representative of the first year peak cooling heat transfer rate. In the second and third years, the difference to the case G2_L2_2.0 is of 3.2% and 2.0%, respectively. On the other hand, the decrease in heating performance is similar to the decrease in cooling performance of case G2_L1_In_2 (-61.1%, -60.0% and -59.5% for the first, second and third year of simulation).

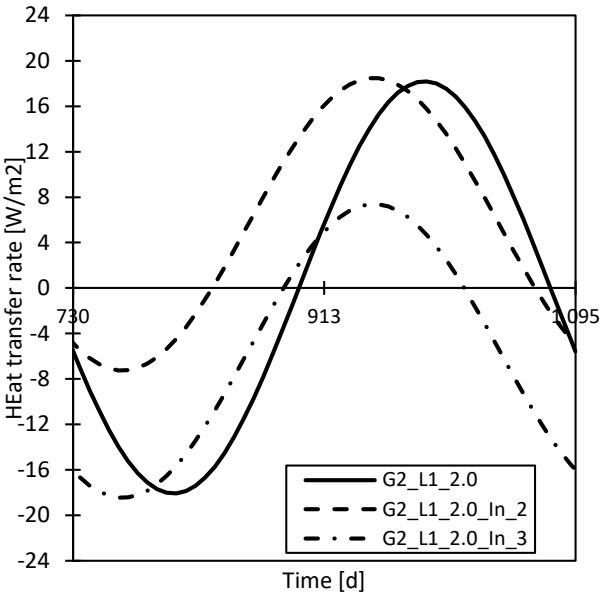

The two cases simulation time was extended to 10 years to check possible losses in the heat transfer rate due to system saturation. However, no significant decrease in performance is observed after 10 years, which indicates that this configuration favours the heat exchange with the interior space that has a variable temperature BC (Int_1) assigned.

4 Conclusions

Based on the previous discussed analyses, the following conclusions can be established:

- Deepest geometries result in lower values of q, as the higher area overcomes the heat power gains, even though the deepest geometries provide a significantly more energy than the shallower geometries;
- The λ_S proves to have a significant positive impact on the heat transfer rate, with an average increase as high as 23.3% between a λ_S of 1.0 W/m K and 3.0 W/m K;
- The conditions on the interior space in contact with the wall also impact the heat transfer rate considerably, with a decrease of almost 13% and 42% when considering low air speeds and insulation between the wall and the space, respectively;
- The temperature at the top BC was found to have a limited impact on the heat transfer rate;
- The unbalanced thermal load imposed by the inlet temperature impact the amount of energy extracted for cooling and heating but the impact seems to stabilise in the first two annual cycles;

References

[1] G. Goetzl, “MUSE – Differences between deep and shallow geothermal energy,” *GeoERA*, 2020. https://geoera.eu/blog/muse-differences-between-deep-and-shallow-geothermal-energy/ (accessed Sep. 25, 2020).

[2] H. Brandl, “Energy foundations and other thermo-active ground structures,” *Geotechnique*, vol. 56, no. 2, pp. 81–122, 2006, doi: 10.1680/geot.2006.56.2.81.

[3] A. Zottl and R. Nordman, “D4.2 /D 2.4. Concept for evaluation of SPF Version 2.2,” pp. 1–18, 2012.

[4] R. Lowe *et al.*, “Final Report on Analysis of Data From Heat Pumps Installed Via the Renewable Heat Premium Payment (RHPP) Scheme,” 2017.

[5] M. Miara, D. Guenther, T. Kramer, T. Oltersdorf, and J. Wapler, “Heat Pump Efficiency - Analysis and Evaluation of Heat Pump Efficiency in Real-life Conditions,” p. 42, 2011.

[6] D. Sterpi, A. Angelotti, O. Habibzadeh-Bigdarvish, and D. Jalili, “Assessment of thermal behaviour of thermo-active diaphragm walls based on monitoring data,” *J. Rock Mech. Geotech. Eng.*, vol. 10, no. 6, pp. 1145–1153, Dec. 2018, doi: 10.1016/j.jrmge.2018.08.002.

[7] A. Angelotti and D. Sterpi, “On the performance of energy walls by monitoring assessment and numerical modelling: a case in Italy,” *Environ. Geotech.*, pp. 1–8, 2018, doi: 10.1680/jenge.18.00037.

[8] C. Xia, M. Sun, G. Zhang, S. Xiao, and Y. Zou, “Experimental study on geothermal heat exchangers buried in diaphragm walls,” *Energy Build.*, vol. 52, pp. 50–55, 2012, doi: 10.1016/j.enbuild.2012.03.054.

[9] M. Sun, C. Xia, and G. Zhang, “Heat transfer model and design method for geothermal heat exchange tubes in diaphragm walls,” *Energy Build.*, vol. 61, pp. 250–259, 2013, doi: 10.1016/j.enbuild.2013.02.017.

[10] T. Amis, C. A. W. Robinson, and S. Wong, “Integrating Geothermal Loops into the Diaphragm Walls of the Knightsbridge Palace Hotel Project,” *Proceeding 11th DFI / EFFC Int. Conf. London*, no. July, p. 10, 2010.

[11] T. Amis, “Energy Piles and Diaphragm Walls,” in *Ground Source Live*, 2011, no. June.

[12] A. Di Donna, F. Cecinato, F. Loveridge, and M. Barla, “Energy performance of diaphragm walls used as heat exchangers,” *Proc. Inst. Civ. Eng. Geotech. Eng.*, vol. 170, no. 3, pp. 232–245, 2017, doi: 10.1680/jgeen.16.00092.

[13] A. Di Donna, F. Loveridge, M. Piemontese, and M. Barla, “The role of ground conditions on the heat exchange potential of energy walls,” *Geomech. Energy Environ.*, vol. 3, 2020, doi: 10.1016/j.gete.2020.100199.

[14] P. J. Bourne-Webb, T. M. Bodas Freitas, and R. A. Da Costa Gonçalves, “Thermal and mechanical aspects of the response of embedded retaining walls used as shallow geothermal heat exchangers,” *Energy Build.*, vol. 125, pp. 130–141, 2016, doi: 10.1016/j.enbuild.2016.04.075.

[15] D. Sterpi, G. Tomaselli, and A. Angelotti, “Energy performance of ground heat exchangers embedded in diaphragm walls: Field observations and optimization by numerical modelling,” *Renew. Energy*, vol. 147, pp. 2748–2760, Mar. 2020, doi: 10.1016/j.renene.2018.11.102.

[16] H. J. G. Diersch, *FEFLOW: Finite element modeling of flow, mass and heat transport in porous and fractured media*, vol. 9783642387. 2014.

[17] M. Barla, A. Di Donna, and A. Santi, “Energy and mechanical aspects on the thermal activation of diaphragm walls for heating and cooling,” *Renew. Energy*, vol. 147, pp. 2654–2663, Mar. 2020, doi: 10.1016/j.renene.2018.10.074.

[18] N. Makasis and G. A. Narsilio, “Energy diaphragm wall thermal design: The effects of pipe configuration and spacing,” *Renew. Energy*, vol. 154, pp. 476–487, 2020, doi: 10.1016/j.renene.2020.02.112.

[19] D. Adam and R. Markiewicz, “Energy from earth-coupled structures, foundations, tunnels and sewers,” *Geotechnique*, vol. 59, no. 3, pp. 229–236, 2009, doi: 10.1680/geot.2009.59.3.229.

[20] IPMA, “Portal do Clima,” 2015. http://portaldoclima.pt/en/ (accessed Jan. 08, 2020).